# Influence of Multiprobe Array Configuration on Planar Wide Mesh Scanning Performance

Jorge Calatayud Maeso*, Celia Fontá Romero*†, Fernando Rodriguez Varela†,
Ana Arboleya Arboleya†, Francesco Saccardi‡, Andrea Giacomini‡, Lars J. Foged‡, Manuel Sierra Castañer*
*Information Processing and Telecommunications Center, ETSI Telecomunicación,
Universidad Politécnica de Madrid, 28040 Madrid, Spain
†Group of Microwave Engineering and Radiocommunication Systems, Universidad Rey Juan Carlos, Madrid, Spain
‡Microwave Vision Group (MVG), Pomezia, Italy
{jorge.cmaeso,manuel.sierra}@upm.es

***Abstract*—This work explores the relevance of multiprobe array design parameters in Planar Wide Mesh (PWM) grids for phase-referenced and reference-less scenarios. This analysis examines the behaviour of the optimisation metric as physical constraints are introduced across multiple multiprobe systems. An extensive comparison of the ideal and retrieved PWS has been conducted to assess the implications of multiprobe parameters in solving the inverse-source problem. This procedure has been repeated to retrieve the phase in a reference-less scenario that uses partially coherent observations in conjunction with PWM grids. Results show that, in the phase-referenced scenario, the optimisation procedure overcomes the limitations introduced by multiprobe constraints. It is concluded that the PWM grids do not constrain the optimal probe spacing. Furthermore, in reference-less scenarios, our results indicate that at least four probes are required for accurate phase retrieval. In the reference-less scenario, we find that certain probe spacing yields less accurate solutions.**

***Index Terms*—antenna measurements, non-redundant sampling, reference-less, multiprobe.**

## I. Introduction

Planar near-field (PNF) scanning [1] offers a distinct advantage for characterising large or reconfigurable antennas, such as Active Phased Arrays (APAs), as it allows the Antenna Under Test (AUT) to remain stationary. Despite this, comprehensively testing modern APAs is bottlenecked by the large scan apertures required to mitigate truncation errors in steered-beam conditions in the traditional near-field-to-far-field transformation.

To mitigate the long measurement times inherent in PNF systems, several techniques have been developed in the literature. Based on the principle that the degrees of freedom of the radiated field are finite, analytical definitions of a non-redundant sampling grid can be found [2], [3]. This methodology was later enhanced by leveraging the Singular Value Decomposition (SVD) of the radiation operator to optimise field-sampling positions in an inverse-source problem [4]. Various function bases, such as Plane Wave Spectrum (PWS) expansions or prolate spheroidal wave functions [4], [5], can be used for this purpose. The measurement time can be further reduced by employing multiprobe systems, which replace slow mechanical scanning with near-instantaneous electronic switching between probes [6]–[8].

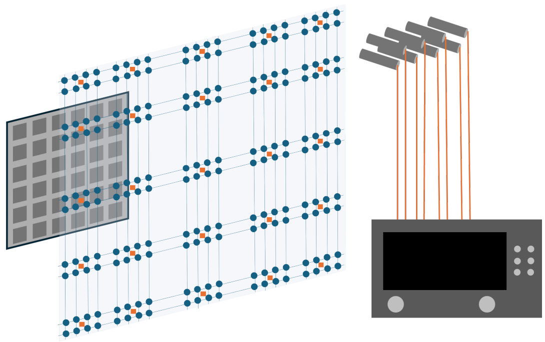

Fig. 1. Measurement scheme for a multiprobe reference-less PWM grid with a coherent receiver

A second major challenge is the prevalence of highly-integrated systems that lack a mechanism for injecting or extracting a phase-referenced signal. A single-scan but complex solution is to recover the signal's phases from partially coherent measurements [9]–[11]. This technique employs a probe array with multiple coherent receivers to establish a phase relationship among simultaneously acquired samples. The inherent coherence between these measurements is then exploited to reduce the total number of unknown absolute phases proportionally to the number of probes. Implementing this technique in a multiprobe system becomes the natural choice as it only requires expanding switchable setups to multiple coherent receivers.

An scheme of the combination of multiprobe arrays with PWM grids and partially coherent measurements is shown in Fig. 1. This work investigates the relationships among the physical design of a multiprobe array, the performance of multiprobe non-redundant sampling grids, and the efficacy of phase recovery using partially coherent observations using PWM sampling grids.

## II. Theoretical Background

### A. Planar Near-Field Measurements

For a given aperture positioned in an XY plane, its radiated field for $z > 0$ can be expanded in PWS components [1] as Eq. 1; being $\vec{E}$ the aperture field, $\vec{P}$ the PWS expansion, $\vec{k}$ the vector wave number and $\vec{r}$ the positioning vector.

$$\vec{P}(k_x, k_y) = \int_{-\infty}^{\infty}\int_{-\infty}^{\infty} \vec{E}_{aut}(x, y) e^{-j(\vec{r}\cdot\vec{k})} dxdy \tag{1}$$

Using the PWS of the antenna, the signal received by a probe along a plane positioned at a given distance $\vec{r} = (x, y, z = d)$ is computed as Eq. 2. It must be noted that the received signal $b$ includes the distortion introduced by the probe's PWS ($\vec{S}(k_x, k_y)$).

$$b(\vec{r}) = \int_{-\infty}^{\infty}\int_{-\infty}^{\infty} \vec{S}(k_x, k_y) \cdot \vec{P}(k_x, k_y) e^{-j(\vec{r}\cdot\vec{k})} dk_x dk_y \tag{2}$$

This Fourier integral formulation (Eqs 1-2) can be discretised and rewritten in a matrix representation as:

$$\mathbf{p} = \mathbf{A_1}\mathbf{e}_{aut} \tag{3}$$

$$\mathbf{b} = \mathbf{A_2}\mathbf{p} \tag{4}$$

Where $\mathbf{A_{1,2}}$ are the two transformation matrices that perform the Fourier integrals. The two discretised equations are then combined into Eq 5 to formulate an inverse source problem that directly relates the field measured samples by the probe ($\mathbf{b}$) to the radiating sources of the AUT $\mathbf{e_{aut}}$. After solving the proposed inverse source problem, the PWS of the AUT can be retrieved using Eq. 3.

$$\mathbf{b} = \mathbf{A_2}\mathbf{A_1}\mathbf{e_{aut}} \Rightarrow \mathbf{b} = \mathbf{A}\mathbf{e_{aut}} \tag{5}$$

### B. Planar Wide Mesh

PWM sampling schemes significantly reduce the number of measurement samples required to capture all the degrees of freedom (DoF) of the aperture fields by optimising the sampling positions $x_m$ [2], [12]. The transformation matrix A is constructed to relate the sampled aperture field and the reduced-order equivalent sources. These positions are used to build a transformation matrix $\mathbf{A}$ that relates the sparse samples to the aperture sources.

An optimisation problem can be formulated to find an optimal grid composed of $M$ samples. The literature presents several metrics to optimise the sampling positions based on the properties of the generated transformation matrix $\mathbf{A}$ [13]. In this work, the Shannon Number (SN) is selected. To simplify the computation of optimal positions, a symmetric mesh with equal rows and columns is considered. This allows us to split the 2D problem into two 1D problems, quadratically reducing the optimisation complexity. In the 1D problem space, the number of optimisation variables can be halved if the AUT is assumed to be positioned centred.

Finally, the optimisation problem to solve for the optimal positioning of $M$ samples is:

$$\begin{aligned} \min_{\mathbf{x}_1,\ldots,\mathbf{x}_M} \quad & \chi = \sum_{n=2}^{N} \frac{\sigma_n(\mathbf{A})}{\sigma_1(\mathbf{A})} \\ \text{s.t.} \quad & \mathbf{A} = f(\mathbf{x}_1, \ldots, \mathbf{x}_M) \\ & 0 \le x_m \le L/2 \quad \forall m = 1, \ldots, M \end{aligned} \tag{6}$$

where $\mathbf{A}$ is the transformation matrix constructed from the $\mathbf{x}$ samples using the Fourier integrals (1-2), $L$ is the desired length of the measurement plane. To estimate the minimum required number of sampling points $M$, the optimisation procedure must be repeated until diminishing returns in SN are observed as $M$ increases. This formulation can be generalised to optimise multiprobe sensing arrays composed of $N$ probes by introducing the concepts of mechanical and electrical positions:

- *Mechanical sample* (MP): Spatial positioning of the center of the multiprobe array, which becomes the variable to optimize. (Orange squares in Fig. 1)
- *Electrical sample* (EP): Field's sampling position calculated as the mechanical position plus the offset of the n-th probe of the array. (Blue dots in Fig. 1)

### C. On the Phase Retrieval from Partial Coherent Probes

In a measurement scenario where there is no reference channel to synchronise the signal source with the receiver, a probe array system can still collect partially coherent samples if each probe's receiver is coherent with the other [9]. This reduces the total unknown phases by the number of probes used. Using this idea, the complex field near-field signal measured at each MP can be decomposed as:

$$|\mathbf{b}| = \begin{bmatrix} |\mathbf{b}_1^T| & |\mathbf{b}_2^T| & \cdots & |\mathbf{b}_n^T| & \cdots & |\mathbf{b}_N^T| \end{bmatrix}^T \tag{7}$$

$$\boldsymbol{\psi} = \begin{bmatrix} \boldsymbol{\psi}_{2,1}^T & \cdots & \boldsymbol{\psi}_{n,1}^T & \cdots & \boldsymbol{\psi}_{N,1}^T \end{bmatrix}^T \tag{8}$$

The measured data consists of the amplitude vector $|\mathbf{b_n}|$ and the relative phase vector $\boldsymbol{\psi_{n,1}}$ (where $\psi_{n,m} = \angle(b_{n,m}/b_{1,m})$). The full complex near-field $\mathbf{b}$ is then reconstructed using Eq. (9), which solves for the unknown absolute phases of the first probe, $\boldsymbol{\psi_1}$. The matrix $\mathbf{B}$ facilitates this by encoding the known amplitude and relative phase data into a series of $N$ vertically concatenated diagonal matrices.

$$\boldsymbol{b} = \boldsymbol{B}\boldsymbol{\psi_1} \tag{9}$$

By joining Eq 5 and Eq 9, the partially coherent observation problem and the reduced order model can be stitched together into a homogeneous linear system of equations defined as:

$$\begin{aligned} (\mathbf{I} - \mathbf{A}\mathbf{A}^{\dagger})\mathbf{B}\boldsymbol{\psi_1} &= 0 \\ \text{s.t}|\boldsymbol{\psi}| &= 1 \end{aligned} \tag{10}$$

where $\mathbf{I}$ is the identity matrix and $\dagger$ calculates the Moore–Penrose inverse. When this formulation is combined with multiprobe PWM grids, solving Eq 10 via non-convex quadratic optimisation yields the best results.

## III. Numerical Experimentation for Multiprobe Arrays

The objective of this research is to determine how the design parameters of a multiprobe array influence PWM grid optimality. The choice of multiprobe array implementation geometry is aimed at commercially viable solutions, often based on linear arrays with a fixed inter-element spacing. For this purpose, a realistic simulation scenario based on a synthetic aperture is performed as follows:

- *AUT*: The AUT consist of a $10\lambda$ by $10\lambda$ aperture with a beam-tilt of -20 degrees and a side lobe level of -15 dB in the analysed measurement plane.
- *Probe Array*: 2, 4, and 8-element probe arrays are simulated, chosen as powers of two for practical implementation with Commercial Off-The-Shelf (COTS) hardware. The inter-element spacing range is within $0.5\lambda$ and $4\lambda$.
- *PNF Setup*: The probe array is located at a distance of $6\lambda$ and scans over a $40\lambda$ wide plane.
- *SNR*: Additive Gaussian White Noise is added to simulate an SNR of 40 dB.

Because the scanning area and the AUT's aperture have equal dimensions in both planes, the optimal mesh will be identical for both rows and columns. As a reference, in a standard single-probe PNF measurement, this scenario would require 80 samples (EPs), spaced by $0.5\lambda$ along each row and column.

### A. Standard Multiprobe PWM

To compare the performance of the different probe array configurations in this scenario, the normalised SN is plotted in Fig. 2. The curves on the graphs show the normalised minimised $\chi_m$ for a set of M mechanical samples. As expected, the number of mechanical samples increases, and the inverse sources problem improves its conditioning until it reaches saturation when all the DoF are sampled [13].

Despite differences in spacing, the optimisation procedure can compensate for this variable by adjusting the overlap between the EPs, achieving a similar system conditioning that is solely determined by the total number of MPs. An example of the PWS retrieved by the three array configurations with a probe separation of $2.5\lambda$ is shown in Fig 3. All retrieved PWS match the reference pattern perfectly. To further illustrate this behaviour, the error (calculated using Eq. 11. ) between the PWS retrieved by solving the inverse source problem and the reference one is shown in Fig 4(a,b,c) as a function of the number of MS and probe spacing in the multiprobe array.

$$\epsilon \; = 20log_{10}\left(\frac{1}{N}\sum\left|P_{CP}^{PWM}(k_x)-P_{CP}^{Ideal}(k_x)\right|\right) \qquad (11)$$

Once the saturation point is reached, additional samples provide greater resilience in accurately solving the inverse source problem. However, the error charts (Fig. 4) show a stable solution for those scenarios close to the saturation point. Therefore, it can be concluded that for a regularly spaced multiprobe array, its spacing is not a critical variable for the PWM procedure. So it can be adjusted as desired to improve probe isolation or the mechanical stability of the array. Table. I illustrates the reduction percentage achieved by the use of PWM grids and multiprobe arrays compared to regular grids. The application of multiprobe arrays to PWM grids achieves a consistent percentage reduction of the MS required to perform the antenna measurement.

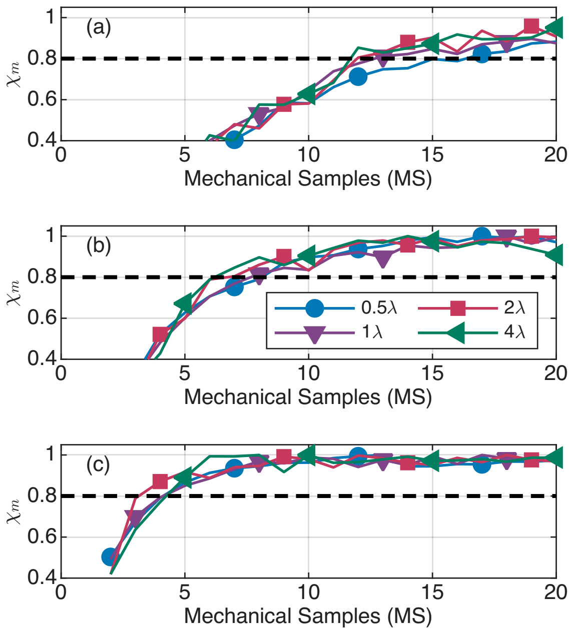


Fig. 2. Normalised minimised Shannon's number for each set of mechanical positions for (a) 2 probes (b) 4 probes (c) 8 probes

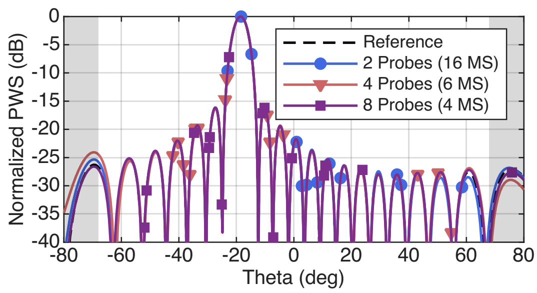


Fig. 3. Retrieved PWS for the standard multiprobe PWM with a probe array spacing of $2.5\lambda$

TABLE I
Comparison of the Number of Mechanical Samples (MS) Required for Regular and PWM Grids as a Function of the Number of Probes Used.

| Probes | MS (Regular Grid) | MS (PWM Grid) | Reduction (%) |
|---|---|---|---|
| 1 | 81 | 27 | 67 |
| 2 | 41 | 16 | 61 |
| 4 | 21 | 7 | 67 |
| 8 | 11 | 4 | 64 |

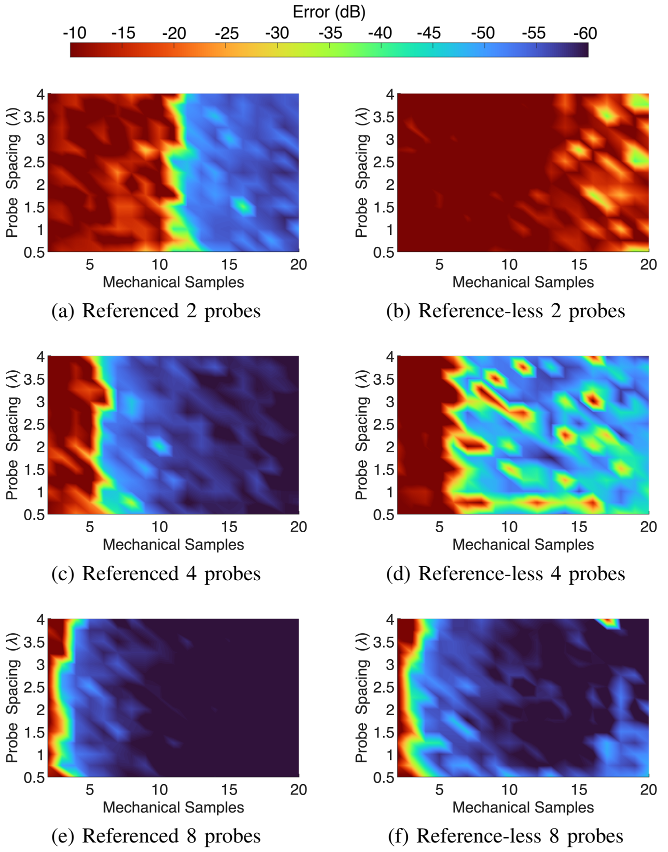


(a) Referenced 2 probes
(b) Reference-less 2 probes
(c) Referenced 4 probes
(d) Reference-less 4 probes
(e) Referenced 8 probes
(f) Reference-less 8 probes

Fig. 4. Error between the ideal PWS and the PWS retrieved from the inverse source problem using the PWM grid for the referenced (With phase) and the reference-less (Relative phase between probes only) scenarios

### B. Reference-less Multiprobe PWM

The reference-less scenario presents a notable challenge, as it requires solving for unknown phases via the optimisation of Eq. 10. The performance of this method is critically dependent on the number of probes in the sensing array. As the probe count increases, the number of unknown phases decreases, simplifying the optimisation problem and improving the accuracy of the reconstructed phase. This leads to a more stable solution for the PWS as shown in Fig. 4(d,e,f).

The performance limitations are most evident in systems with fewer probes. A two-probe array is unfeasible, as increasing the number of mechanical samples (MS) fails to reduce the retrieval error. Fig. 5 shows how the two-probe configuration fails to retrieve most of the PWS. Expanding the array to four probes allows the solution to converge for configurations with more than 5 MS (Fig. 4d). However, performance is inconsistent and highly dependent on probe spacing. While optimal spacings of $1\lambda$, $1.75\lambda$, and $2.5\lambda$ can achieve an error below -40 dB, other configurations fail to yield a stable solution.

Finally, the eight-probe array achieves a retrieval accuracy comparable to that of the phase-referenced measurement (Fig. 4f). For most configurations using more than 4 MS, this array consistently retrieves the PWS with an error below -

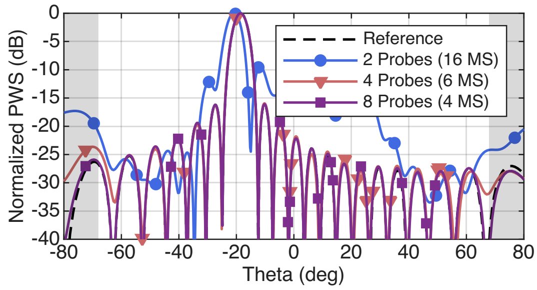


Fig. 5. Retrieved PWS for the reference-less multiprobe PWM with a probe array spacing of $2.5\lambda$

45 dB. This result confirms that minimising the number of unknown variables in Eq. 10 is the key to achieving robust and accurate results in a reference-less measurement. However, oversampling the measurement plane may create numerical instabilities, as shown by the red spot in Fig. 4f for a spacing of $4\lambda$ and 17 MS.

### C. Broadband Performance of PWM Grids with Multiprobe Systems

To validate the performance of the proposed reduced-order sampling grids for multifrequency acquisitions, we simulate a shared-aperture phased array operating across an octave bandwidth. This approach is motivated by state-of-the-art commercial systems, such as the MVG 1-18 GHz multiprobe array [14].

The simulation operates at two frequencies and relies on electrical scaling of the fixed physical hardware. The key parameters are:

- Operating Frequencies: 16 GHz (Ku-band) and 8 GHz (X-band), simulating a realistic dual-band aperture antenna.
- Aperture Scaling: A physical aperture that is electrically $10\lambda$ at 16 GHz is scaled to $5\lambda$ at 8 GHz.
- Probe Spacing Scaling: This spacing is defined at the upper frequency to be in the range of $2\lambda$ to $4\lambda$. At the lower frequency, this same physical spacing corresponds to an electrical separation of $1\lambda$ to $2\lambda$. The number of probes has been fixed to four as a compromise between the system's complexity and the reference-less capabilities.

The PWS of the scaled scenario for Fig. 3 and Fig. 5 is shown in Fig. 6. The recovered pattern for this scenario mimics the performance of the previous results. A broader picture of multiple configurations is shown in Fig. 7, which shows the error metrics of the retrieved pattern across all possible scaled configurations. For the referenced scenario, the error exhibits behaviour highly similar to that in 4c. In contrast, the reference-less case shows improvement over the upperband case, with instability in the phase retrieval process significantly reduced and no configuration failing at the phase retrieval problem.

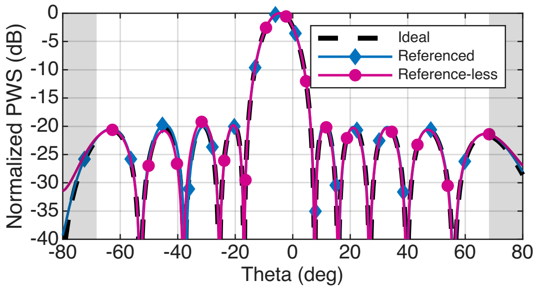


Fig. 6. Retrieved PWS for the broadband scenario (AUT aperture of $5\lambda$) using a four-probe phased array with $1.25\lambda$ spacing and 6 MS

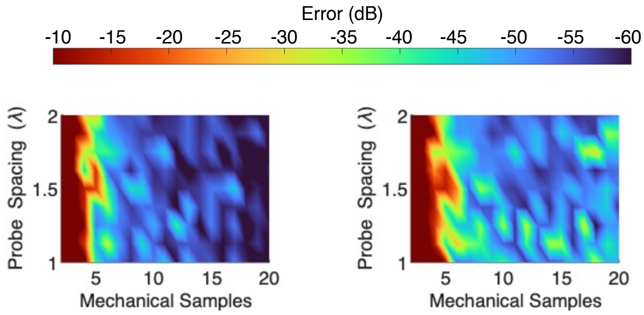


(a) Referenced 4 probes (b) Reference-less 4 probes

Fig. 7. Error of the retrieved pattern for the broadband scenario using a four-probe linear array

## IV. Conclusion

This work has explored the impact of the design variables of multiprobe systems in conjunction with PWS sampling grids and their natural application to the reference-less scenarios. Through numerical simulation of measurement scenarios using a synthetic-aperture model, it has been confirmed that the spacing between elements in the multiprobe array does not directly affect the performance of the PWM grids, provided it is accounted for in the optimisation procedure. For a broadband scenario, this has also been demonstrated to be true. The reduction of samples achieved due to the multiprobe array is proportionally consistent between regular and PWM grids.

The reference-less scenario reveals a much more complex reality in which the number of selected probes directly affects algorithm performance. In conjunction with PWM grids, using fewer than four probes yields highly inaccurate results in the phase reconstruction from partially coherent samples. The numerical instability of this phase-retrieval method on oversampled grids persists.

## Acknowledgment


This work was supported by the projects Sub-Terahertz Antenna Technologies for Communications In the Road to 6G–UPM-STAIRto6G (PID2023-151385OA-I00), funded by MICIU/AEI/10.13039/501100011033 and FEDER, EU, MICIN, AEI and the European Union NextGenerationEU/PRTR under Project TED2021-131975AI00/AEI/10.13039/501100011033 (ANTHEM5G) and Advancing Radio Technologies for the Evolution towards 6G – UPM-ARTE6G (PID2024-157242OB-C41), funded by MICIU/AEI/10.13039/501100011033


## References


[1] S. Gregson, J. McCormick, and C. Parini, *Principles of Planar Near-Field Antenna Measurements*. IET Digital Library, Jan. 2007. [Online]. Available: https://digital-library.theiet.org/content/books/ew/pbew053e

[2] O. Bucci and G. Franceschetti, "On the spatial bandwidth of scattered fields," *IEEE Transactions on Antennas and Propagation*, vol. 35, no. 12, pp. 1445–1455, Dec. 1987, conference Name: IEEE Transactions on Antennas and Propagation.

[3] O. Bucci, C. Gennarelli, and C. Savarese, "Representation of electromagnetic fields over arbitrary surfaces by a finite and nonredundant number of samples," *IEEE Transactions on Antennas and Propagation*, vol. 46, no. 3, pp. 351–359, Mar. 1998. [Online]. Available: https://ieeexplore.ieee.org/document/662654

[4] F. D'Agostino, F. Ferrara, C. Gennarelli, R. Guerriero, and M. Migliozzi, "An SVD-Based Approach to Reconstruct the Planar Wide-Mesh Scanning NF Data From Inaccurately Probe-Positioned Samples," *IEEE Antennas and Wireless Propagation Letters*, vol. 17, no. 4, pp. 641–644, Apr. 2018, conference Name: IEEE Antennas and Wireless Propagation Letters.

[5] A. Capozzoli, L. Celentano, C. Curcio, A. Liseno, and S. Savarese, "Optimized Trajectory Tracking of a Class of Uncertain Systems Applied to Optimized Raster Scanning in Near-Field Measurements," *IEEE Access*, vol. 6, pp. 8666–8681, 2018, conference Name: IEEE Access.

[6] F. Rodríguez Varela, M. J. López Morales, R. Tena Sánchez, A. T. Muriel Barrado, E. de la Fuente González, G. Posada Quijano, C. Zarzuelo Torres, M. Sierra Pérez, and M. Sierra Castañer, "Multi-Probe Measurement System Based on Single-Cut Transformation for Fast Testing of Linear Arrays," *Sensors*, vol. 21, no. 5, p. 1744, Jan. 2021, publisher: Multidisciplinary Digital Publishing Institute. [Online]. Available: https://www.mdpi.com/1424-8220/21/5/1744

[7] F. R. Varela, M. S. Castañer, F. Saccardi, L. Scialacqua, and L. Foged, "Planar Wide Mesh Scanning using Multi-Probe Systems," in *2023 Antenna Measurement Techniques Association Symposium (AMTA)*, Oct. 2023, pp. 1–5, iSSN: 2474-2740. [Online]. Available: https://ieeexplore.ieee.org/abstract/document/10293361

[8] F. Saccardi, N. Gross, P. Iversen, K. Hassett, J. Hartzell, T. Schellenberg, G. Pinchuk, R. Braun, L. Shmidov, S. Solomon, M. He, X. Bland, and L. J. Foged, "Fast Multi-Probe Planar Near Field Measurements With Full Probe Compensation," in *2021 15th European Conference on Antennas and Propagation (EuCAP)*, Mar. 2021, pp. 1–5. [Online]. Available: https://ieeexplore.ieee.org/document/9411444

[9] A. Paulus, J. Knapp, J. Kornprobst, and T. F. Eibert, "Reliable Linearized Phase Retrieval for Near-Field Antenna Measurements With Truncated Measurement Surfaces," *IEEE Transactions on Antennas and Propagation*, vol. 70, no. 8, pp. 7362–7367, Aug. 2022, conference Name: IEEE Transactions on Antennas and Propagation. [Online]. Available: https://ieeexplore.ieee.org/document/9696234

[10] F. Rodríguez Varela, J. C. Maeso, X. Sun, B. G. Iragüen, and M. S. Castañer, "Single-Cut Phaseless Near-Field Measurements Using Two Probes," *IEEE Transactions on Antennas and Propagation*, vol. 72, no. 2, pp. 1935–1940, Feb. 2024. [Online]. Available: https://ieeexplore.ieee.org/document/10346999/

[11] F. R. Varela, M. S. Castañer, F. Saccardi, A. Giacomini, and L. Foged, "Planar Near-Field Phaseless Measurements Using Multi-Probe Arrays," in *2024 18th European Conference on Antennas and Propagation (EuCAP)*, Mar. 2024, pp. 1–5. [Online]. Available: https://ieeexplore.ieee.org/abstract/document/10501756

[12] N. Mézières, M. Mattes, and B. Fuchs, "Antenna Characterization From a Small Number of Far-Field Measurements via Reduced-Order Models," *IEEE Transactions on Antennas and Propagation*, vol. 70, no. 4, pp. 2422–2430, Apr. 2022. [Online]. Available: https://ieeexplore.ieee.org/document/9573335

[13] A. Capozzoli, C. Curcio, and A. Liseno, "Different Metrics for Singular Value Optimization in Near-Field Antenna Characterization," *Sensors*, vol. 21, no. 6, p. 2122, Jan. 2021, number: 6 Publisher: Multidisciplinary Digital Publishing Institute. [Online]. Available: https://www.mdpi.com/1424-8220/21/6/2122

[14] "SpeedProbe DL : Measurement Probes and Feeds." [Online]. Available: https://www.mvg-world.com/en/products/antennas/measurement-probes-and-feeds/speedprobe-dl